

Electron and nuclear spin properties of the nanohole-filled GaAs/AlGaAs quantum dots

Ata Ulhaq,^{*,†} Qingqing Duan,[†] Fei Ding,[‡] Eugenio Zallo,^{‡,¶} Oliver G. Schmidt,[‡] Maurice S. Skolnick,[†] Alexander I. Tartakovskii,[†] and Evgeny A. Chekhovich^{*,†}

Department of Physics and Astronomy, University of Sheffield, Sheffield, S3 7RH, United Kingdom., Institute for Integrative Nanoscience, IFW Dresden, Helmholtz str. D-01069, Dresden, Germany., and Paul-Drude-Institut für Festkörperelektronik, Hausvogteiplatz 5-7, 10117 Berlin, Germany

E-mail: a.ulhaq@sheffield.ac.uk; e.chekhovich@sheffield.ac.uk

Abstract

GaAs/AlGaAs quantum dots grown by *in situ* droplet etching and nanohole infilling offer a combination of strong charge confinement, optical efficiency, and spatial symmetry required for polarization entanglement and spin-photon interface. Here we study spin properties of such dots. We find nearly vanishing electron g -factor ($g_e < 0.05$), providing a route for electrically driven spin control schemes. Optical manipulation of the nuclear spin environment is demonstrated with nuclear spin polarization up to 60% achieved. NMR spectroscopy reveals the structure of two types of quantum dots and yields the small magnitude of residual strain $\epsilon_b < 0.02\%$ which nevertheless leads to long nuclear spin lifetimes exceeding 1000 s. The stability of the nuclear spin environment is advantageous for applications in quantum information processing.

Central spin in semiconductor quantum dots is a prime candidate for applications in quantum information technologies.^{1,2} It is relatively isolated from the solid state effects and at the same time is accessible for coherent manipulation and can be interfaced optically. The coherence in this system is mainly limited by the hyperfine coupling with the nuclear spin bath.^{3,4} Single spin qubit manipulation in these structures, therefore, demands an auxiliary control over nuclear spin environment. Such control can be realized by maximizing polarization of $10^4 - 10^5$ nuclei in a single quantum dot,⁵⁻⁷ enabling the formation of well-defined nuclear spin states and in effect reducing the influence of the nuclear field fluctuations.^{8,9}

Central spin manipulation in semiconductor quantum dot (QD) system using resonant ultrafast optical pulses^{10,11} has been demonstrated but scalability in such schemes is challenging. An

alternative approach is to induce controlled spin rotation by manipulating the coupling to the external magnetic field.¹² This can be achieved by electrical modulation of the g -factor. However, such scheme critically depends on the ability to change the sign of g , thus requiring quantum dots with close to zero electron or hole g -factor.^{13,14}

Self-assembled InGaAs/GaAs QD has been the primary system of choice for spin studies over the last two decades, as quantum confinement in monolayer-fluctuation GaAs/AlGaAs dots is too weak. Only recently the potential of droplet epitaxial (DE) grown GaAs QDs has been identified.¹⁵⁻¹⁷ In particular nanohole-filled droplet epitaxial (NFDE) dots formed by *in situ* etching and nanohole infilling¹⁸ provide confinement and excellent optical efficiency, while on the other hand exhibiting high symmetry not achievable previously in self-assembled dots.¹⁹ Such unique com-

combination of properties make NFDE dots ideal candidates for polarization entanglement and spin-photon interface.²⁰ This system has already exhibited an efficient interface between rubidium atoms and a quantum dot.²¹ However, the understanding of the spin properties in such quantum dots is still lacking.

Here we use optical and nuclear magnetic resonance (NMR) spectroscopy to study the properties of the single charge spins and nuclear spin environment in NFDE grown GaAs/AlGaAs QDs. Magneto-photoluminescence measurements reveal close-to-zero electron g -factor, due to the electron wavefunction overlap with the AlGaAs barrier. We demonstrate efficient dynamic nuclear polarization (DNP) as large as 60 %. By measuring the excitation wavelength dependence we identify three mechanisms of DNP: (i) via optical excitation of the quantum well states, (ii) via resonant optical excitation of the dot ground or excited states, and (iii) via resonant excitation of the neighboring dot made possible by inter-dot charge tunneling. Radio frequency (rf) excitation is used to measure NMR spectra revealing the presence of small ($< 0.02\%$) residual biaxial strain. Surprisingly, we observe two sub-ensembles of QDs one with compressive and another with tensile strain along the growth axis: this allows us to identify these two types of dots as formed in the nanoholes and at the rims of the nanoholes respectively. We show that small residual strain results in very stable nuclear spin bath with nuclear spin relaxation times > 1000 s, previously achievable only in self-assembled dots. The properties of the NFDE quantum dots revealed in this study make them a favorable system for electrical spin qubit manipulation with a potential for minimized decoherence effects from the nuclear spin bath.

Single dot photoluminescence (PL) spectroscopy is performed with a confocal setup which collects PL at low temperature ($T \approx 4.2$ K) from a $\sim 1 \mu\text{m}$ spot. Magnetic fields up to 10 T along sample growth axis (Faraday geometry) are employed in this study. The polarization degree of the nuclear spins is probed by measuring the hyperfine shifts in the Zeeman splitting of the quantum dot PL. Nuclear spin polarization and NMR spectroscopy studies are performed using the methods described in Reference.²²

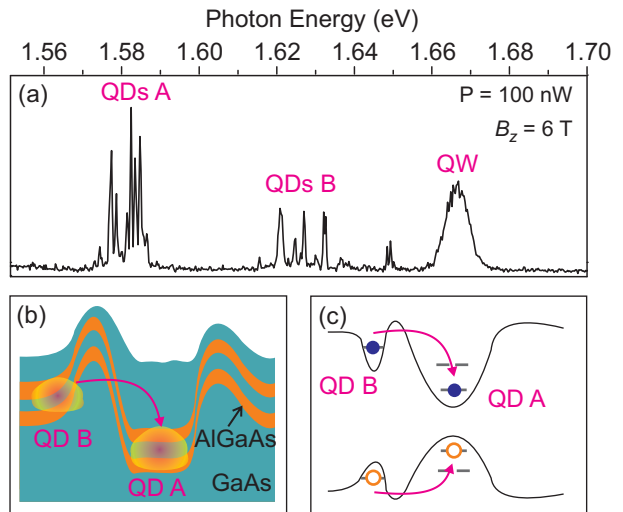


Figure 1: (a) Low temperature photoluminescence spectrum showing emission of two types of quantum dots (A and B) and a quantum well (QW) measured under non resonant excitation ($E_{\text{laser}} = 1.96$ eV) at $B_z = 6$ T. (b) Schematic diagram showing the structure of *in situ* nanohole infilled droplet epitaxial QDs. The deposited GaAs causes formation of a dot inside the nanohole (QD type A), additional dots (type B) can be formed at the edge of the nanohole. (c) Schematic bandstructure of a nanohole infilled dots A and type B. Arrows depict a possible exciton tunneling from dot B to dot A.

A typical broad PL spectrum of the studied structure under non-resonant excitation ($E_{\text{laser}} = 1.96$ eV) is shown in Fig. 1(a) at $B_z = 6$ T. Apart from the quantum well (QW) emission at $E = 1.67$ eV, two spectral distributions of QD emission are observed at $E \approx 1.58$ eV (type A dots) and $E \approx 1.63$ eV (type B). The structure of the QD sample used in this study based on previous AFM measurements¹⁸ is shown schematically in Fig. 1(b). Inverted pyramid dot formation is caused by infilling with GaAs of the *in situ* etched nanoholes in AlGaAs. These dots are responsible for emission at $E \approx 1.58$ eV (QDs type A). The topology of the nanohole allows the formation of smaller dots. As we show based on NMR spectroscopy measurements such dots are formed at the edges of the nanohole. Such dots have shallower potential and give rise to emission at higher energy $E \approx 1.63$ eV (QDs type B).

Emission from a QD is a result of recombination of an electron with spin up \uparrow (or spin down \downarrow) and a hole with spin up \uparrow (or spin down \downarrow) along O_z axis

(parallel to magnetic field B_z). An electron-hole pair can form either a "bright" exciton $|\uparrow\downarrow\rangle$ ($|\downarrow\uparrow\rangle$) with spin projection $+1$ (-1) or optically forbidden "dark" exciton^{23,24} $|\uparrow\uparrow\rangle$ ($|\downarrow\downarrow\rangle$) with spin projection $+2$ (-2). In QDs with non-ideal symmetry, the exchange interaction mixes the bright and dark states²³ and hence the dark states gain small oscillator strength and can be observed in QD PL at low excitation powers.

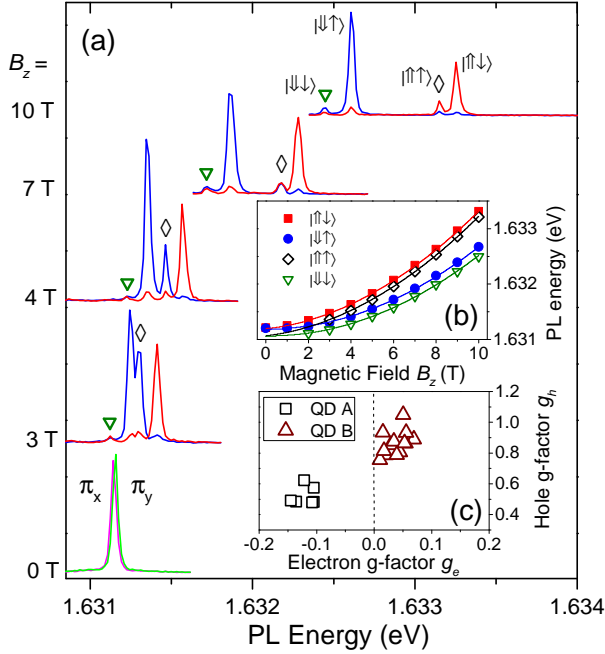


Figure 2: (a) Magnetic field B_z dependence of PL emission from bright and dark excitons in a quantum dot B1 under σ^+ low power ($P_{exc} = 200$ nW) excitation. Red (blue) lines correspond to spectra recorded in σ^+ (σ^-) polarized detection, while green and magenta correspond to spectra recorded in linear polarizations (π_x , π_y) at $B_z = 0$. The diamonds (\diamond) and triangles (∇) indicate the weak peaks corresponding to $|\uparrow\uparrow\rangle$ and $|\downarrow\downarrow\rangle$ dark excitons, respectively. The two intense peaks correspond to $|\uparrow\downarrow\rangle$ and $|\downarrow\uparrow\rangle$ bright exciton. (b) PL energies of 'dark' (open symbols) and 'bright' (full symbols) exciton peaks from (a). The solid lines show fit to the data yielding the electron (hole) g -factor $g_e = 0.05$ ($g_h = 0.86$) and diamagnetic shift $\kappa = 21.8 \mu\text{eV}/\text{T}^2$. (c) Electron (g_e) and hole (g_h) g -factors measured for several QDs type A (squares) and QDs B (triangles) from the same sample.

Figure 2(a) presents a series of PL spectra of QD B1 measured at low excitation power and different B_z . The emission of both dark excitons can be observed at finite B_z : the emission lines are marked with \diamond for $|\uparrow\uparrow\rangle$ and ∇ for $|\downarrow\downarrow\rangle$ exciton. A finger-

print feature of a "dark" exciton is its enhanced emission when it anticrosses with a bright state.²³ This is observed in Fig. 2(a) for the $|\uparrow\uparrow\rangle$ exciton: at $B_z = 3$ T it has enhanced emission in σ^- polarization due to the mixing with $|\downarrow\uparrow\rangle$, while at $B_z = 10$ T the enhanced emission in σ^+ polarization is caused by mixing with $|\uparrow\downarrow\rangle$ bright exciton.

The PL peak energies are shown in Fig. 2(b) by the symbols. The fitting is shown by solid lines. From the fit we find the electron and hole Landè g -factors along Oz axis g_e and g_h and the diamagnetic shift coefficient κ . We have performed magneto-PL measurements for a set of different individual dots of both type A and B from the same sample. The extracted electron and hole g -factors are plotted in Fig. 2(c). Surprisingly, for QDs B, g_e have close-to-zero values with an average of $g_e \sim +0.05$, an order of magnitude smaller than for GaAs/AlGaAs QDs formed by natural fluctuation of the quantum well width.^{25,26} QDs of type A also have small (and negative g -factors) $g_e \approx -0.1$. The values of diamagnetic shift κ is $16 - 22 \mu\text{eV}/\text{T}^2$ for both type A and B dots, which is larger than in natural GaAs/AlGaAs QDs ($10 \mu\text{eV}/\text{T}^2$, Ref.²⁵) and DE-grown GaAs/AlGaAs QDs obtained by crystallization of Ga droplets ($4 - 8 \mu\text{eV}/\text{T}^2$, Ref.¹⁶). We attribute large diamagnetic shifts of the studied NFDE QDs to their larger lateral dimensions resulting in weaker confinement:²⁷ a typical nanohole size is ~ 65 nm (Ref.¹⁸) compared to droplet size ~ 40 nm in DE-grown dots.²⁸

Confinement of the charges has also a strong impact on the Landè g -factors.²⁹ Due to the large lateral size of the wavefunction in the NFDE dots, the g -factor of the semi-confined electron can be approximated as an average of the g -factors in the dot and in the barrier materials weighted by the probability of finding the charge in them.^{30,31} Since electron g -factor is negative in GaAs and positive in AlGaAs^{32,33} we ascribe the nearly zero g_e observed in the studied NFDE dots to significant penetration of the electron wavefunction into the AlGaAs barrier.^{29,34} This conclusion agrees with the observation of smaller g_e in QDs A [Fig. 2(a)] that have smaller PL energy and hence stronger exciton confinement.

Based on our observation of very small $g_e \sim 0.05$ we expect that nanohole etching and subsequent

infilling process can be optimized to obtain QDs of either type A or type B with $g_e \approx 0$. The g_e in a QD can be tuned via electric field.³⁵ Therefore, adding electrodes to NFDE QD structures with $g_e \approx 0$ would allow coherent rotation with an access to an arbitrary part of the electron spin Bloch sphere by switching the value of the electric field.^{12,36} The advantage of this approach is that a large number of QD spin qubits can be controlled independently by multiple electrodes on the same semiconductor chip. This would allow for scalability - the key requirement on the way for practical implementation of quantum information processing devices.

Since in III-V semiconductors the electron spin is coupled to the nuclear spin environment via hyperfine interaction, it is important to understand the properties of the nuclear spin bath and establish the techniques for its manipulation. To monitor the polarization of the QD nuclei we measure the splitting $\Delta E_{|\uparrow\downarrow\rangle,|\downarrow\uparrow\rangle}$ between the Zeeman components ($|\uparrow\downarrow\rangle$ and $|\downarrow\uparrow\rangle$) of the bright exciton. The Overhauser shift E_{OHS} is the change in $\Delta E_{|\uparrow\downarrow\rangle,|\downarrow\uparrow\rangle}$ and characterizes the degree of nuclear spin polarization.

We start by investigating the dynamic nuclear polarization (DNP) under optical pumping, in particular the dependence on the energy of the laser excitation E_{laser} . Fig. 3(a) shows PL spectrum of QD A2 used in these experiments; the emission from the type B dots is also observed. Photoluminescence excitation (PLE) spectrum of QD A2 under excitations with both circular polarizations at low optical power of $2 \mu\text{W}$ is presented in Fig. 3(c). The PLE data reveals sharp peaks for E_{laser} up to $\sim 1.61 \text{ eV}$, $\sim 25 \text{ meV}$ above QD A2 ground state energy $\sim 1.585 \text{ eV}$ - these can be ascribed to the excited states of the QD A2. Above $E_{\text{laser}} \sim 1.61 \text{ eV}$ the PLE trace has a broad background. We attribute this to the large lateral size of the type A quantum dot resulting in high spectral density of the excited states merging into a continuum. However, in addition to this broad background there is a set of sharp PLE peaks observed above $E_{\text{laser}} = 1.63 \text{ eV}$. These have energies close to the energies of the PL peaks of the type B quantum dots, suggesting that there is an efficient mechanism for injecting electron-hole pairs into A dots via the excitation of the B dots as shown schematically in Fig. 1(c).

In addition to PLE spectroscopy we have measured the nuclear polarization E_{OHS} as a function of E_{laser} . The red (blue) line in Fig. 3(b) shows positive (negative) E_{OHS} induced in QD A2 under σ^+ (σ^-) polarized high power ($P = 500 \mu\text{W}$) optical excitation. (The measurement was performed with pump-probe techniques²²). The results allow to identify at least three mechanisms of DNP: (i) It can be seen that the highest efficiency DNP with $|E_{\text{OHS}}| \geq 70 \mu\text{eV}$ is achieved for $E_{\text{laser}} \sim 1.675 \text{ eV}$ corresponding to the QW states - this is similar to DNP via QW states in fluctuation GaAs quantum dots^{6,37} and DNP via the wetting layer states in self-assembled dots.^{7,25} (ii) A series of sharp peaks between $E_{\text{laser}} = 1.585 - 1.60 \text{ eV}$ is observed correlated with the PLE peaks in Fig. 3(c). These correspond to DNP via resonant optical excitation either of the QD A2 ground state or excited states (e.g. p -shell). Such mechanism is also well known from the studies on self-assembled quantum dots.³⁸⁻⁴¹ Similar to the case of PLE, the non-zero background E_{OHS} at all $E_{\text{laser}} > 1.60 \text{ eV}$ is ascribed to nearly continuum spectrum of the excited states of the NFDE QDs with large lateral dimensions. (iii) Finally, a set of sharp peaks is observed in Fig. 3(b) at $E_{\text{laser}} = 1.63 - 1.66 \text{ eV}$. These peaks are strongly correlated to both PLE and PL peaks of the type B QDs, suggesting that DNP in one dot (of type A) can be produced by optical excitation of another dot (of type B). Such mechanism has not been reported previously and is unique to the NFDE QDs.

In order to understand the mechanism of the inter-dot DNP we perform high-resolution spectroscopy as shown in Figs. 3(d-f) where we focus on the range of energies around QD B2 ground excitonic state. Vertical dashed lines show that with high accuracy there is a direct correspondence between the peaks in PLE (f) and DNP (e) spectra, confirming that the DNP in QD A2 is a result of the resonant optical electron-hole injection into the dot. One doublet of the circularly polarized PLE and DNP peaks at 1.632 eV can be attributed to the Zeeman doublet of the QD B2 observed in PL (d). This allows to explain the mechanism of the inter-dot DNP: under resonant optical excitation an exciton is generated in QD B2. With a finite probability this exciton can tunnel into QD A2, where it can exchange electron spin with a nucleus [re-

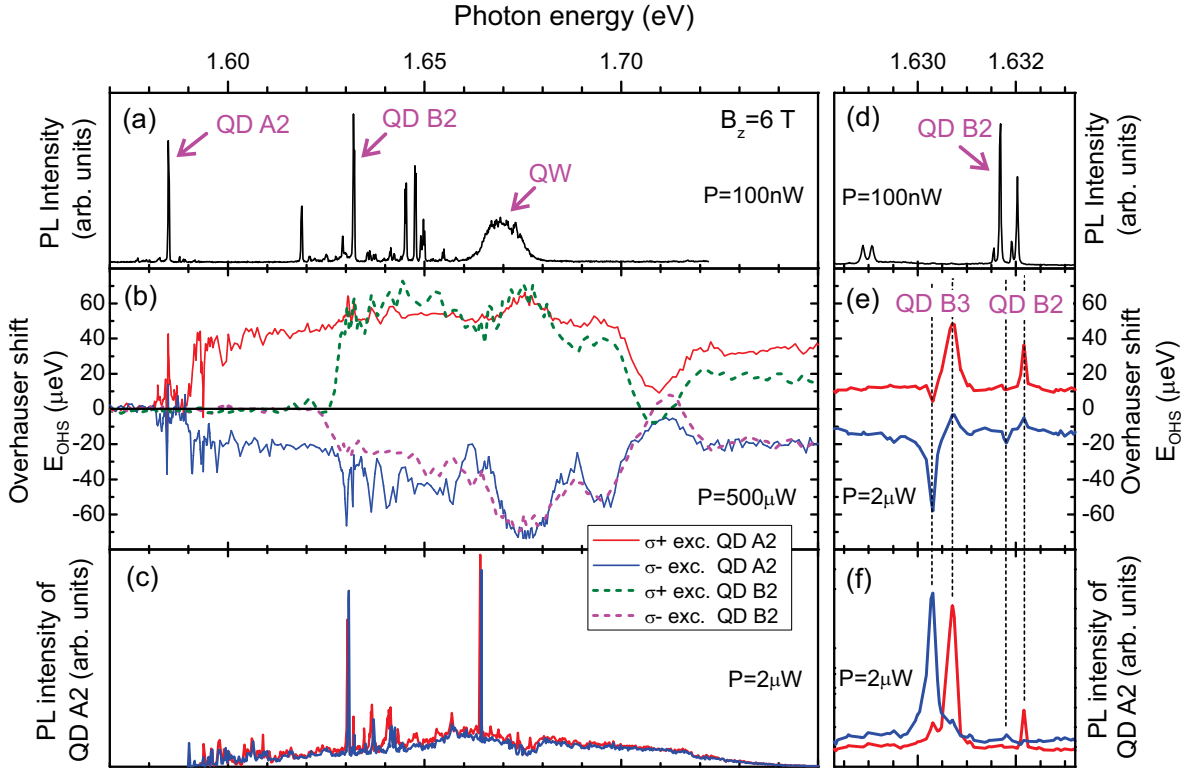


Figure 3: Polarization dependent PL, PLE, and DNP spectroscopy on GaAs QDs at $B_z = 6$ T. (a) PL spectrum showing QW, QD A2 and QD B2 emission under non resonant excitation ($E_{\text{laser}} = 1.96$ eV). (b) Overhauser shift measured on dots A2 (blue line for σ^- and red line for σ^+ excitation) and B2 (magenta line for σ^- and green line for σ^+ excitation) as a function of the laser excitation energy E_{laser} . (c) PL emission magnitude of QD A2 (red for σ^+ and blue for σ^- excitation) as a function of E_{laser} . (d) High resolution PL spectrum of QD B2. (e) Low power DNP measured on QD A2 as E_{laser} is scanned close to QD B2 resonance. (f) Zoomed-in view of (c).

sulting in a DNP peak in Fig. 3(e)] and then recombine [resulting in a PLE peak in Fig. 3(f)]. We note that the PL peaks of QD B2 in Fig. 3(d) are red-shifted by $150 \mu\text{eV}$ from the corresponding PLE and DNP peaks in Figs. 3(e,f). We ascribe this to Pauli blockade:⁴² the PLE absorption in QD B2 is observed only when QD A2 is empty, by contrast the PL from QD B2 can only be observed when QD A2 is occupied with an exciton, preventing further exciton tunneling from QD B2 as well as shifting the ground state energy of QD B2.

On the other hand, the much stronger PLE and DNP doublets at 1.630 eV seemingly have no PL lines from type B QD related to them. This however, can be understood if we assume that such QD (that we denote as B3) exists but has much larger tunneling rate compared to QD B2. Thus the excitons from QD B3 tunnel into QD A2 before they can recombine, as a result the PL from QD B3 is suppressed while PL and DNP in QD A2 are enhanced. We have also measured the DNP in QD

B2 as a function of E_{laser} as shown in Fig. 2(b) by the dashed lines. Importantly there is no DNP in QD B2 when exciting QD A2: we thus conclude that the nuclear spin diffusion between the dots is negligible and the inter-dot DNP in QD A2 under resonant optical excitation of QD B2 is indeed due to the tunneling of the excitons.

Upon examining several QDs from the same sample we found that the results presented in Fig. 3 are well reproduced in other dots. The DNP in dots type A induced via its resonant pumping is found to be as large as $|E_{\text{OHS}}| \approx 50 \mu\text{eV}$. The DNP induced via optical pumping into the QW or via tunneling from type B dots is noticeably larger $|E_{\text{OHS}}| \approx 85 \mu\text{eV}$, corresponding to polarization degrees of $\sim 60\%$. However, the DNP via inter-dot tunneling may have an advantage since it allows for a selective control of the nuclear polarization in individual dots, while non-resonant excitation of the QW polarizes nuclei in all dots within the laser spot.⁴³

The ability to induce large DNP allows us to

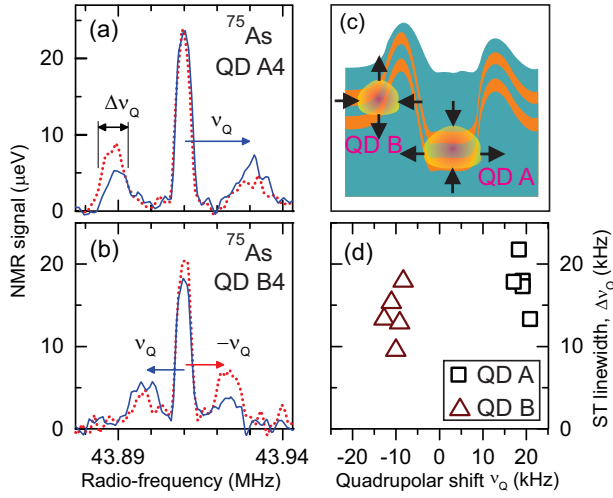


Figure 4: Nuclear magnetic resonance spectrum of ^{75}As nuclei measured on QD A4 (a) and QD B4 (b) under σ^+ (red lines) and σ^- (blue lines) optical nuclear spin pumping. The satellite transitions (STs) are separated from the central transition (CT) by the strain induced quadrupolar shift ν_Q . The central transition is resolution limited while the ST width is $\Delta\nu_Q$. (c) Schematic showing the strain profile in dots A and B with black arrows indicating the strain directions for both dots as deduced from the NMR spectra in (a) and (b). (d) Mean quadrupolar shifts ν_Q and ST broadening $\Delta\nu_Q$ measured for several QDs type A (squares) and B (triangles).

perform nuclear magnetic resonance (NMR) spectroscopy in order to investigate the QD structural properties.²² Figs. 4(a) and (b) show NMR spectra of the ^{75}As spin $I = 3/2$ isotope for QDs A4 and B4, respectively. The spectra contain a narrow (resolution limited) central peak corresponding to the nuclear spin $-1/2 \leftrightarrow +1/2$ central transition (CT). Two satellite transitions (STs) $\pm 3/2 \leftrightarrow \pm 1/2$ are shifted by frequency $\mp \nu_Q$ from the CT. The non-zero ν_Q reveals the presence of a biaxial elastic strain, even though the GaAs/AlGaAs structures are expected to be nearly lattice-matched.¹⁵

In order to quantify the strain in QDs we first note an asymmetry observed in the NMR spectra of Figs. 4(a,b): under the σ^+ optical pumping the low-frequency (high-frequency) ST of QD A4 (B4) has increased amplitude. As σ^+ light enhances the NMR signal of the $-3/2 \leftrightarrow -1/2$ ST,²² we conclude that QDs A4 and B4 have opposite signs of the quadrupolar shifts: $\nu_Q > 0$ for QD A4 and $\nu_Q < 0$ for QD B4. NMR mea-

surements on several individual dots shown in Fig. 4(d) reveal systematic positive values $\nu_Q \approx +20$ kHz for dots type A (squares) and negative values $\nu_Q \approx -10$ kHz for dots type B (triangles). The ST half-widths $\Delta\nu_Q$, reflecting the inhomogeneous distribution of ν_Q within the dot are found to vary in the range $\Delta\nu_Q \sim 10 - 20$ kHz.

Pure hydrostatic strain does not cause nuclear quadrupolar shifts. But under a uniaxial strain of magnitude ϵ_b and with major axis parallel to magnetic field (along Oz), the quadrupolar shift reads as:

$$\nu_Q = \frac{3eQS_{11}\epsilon_b}{2hI(2I-1)}, \quad (1)$$

where Q is the nuclear quadrupolar moment ($\approx 0.31 \times 10^{-28}$ m² for ^{75}As), $|S_{11}| \approx 3.9 \times 10^{22}$ V/m² is the gradient elastic tensor for ^{75}As in bulk GaAs (the sign of S_{11} is undefined),⁴⁴ e is electron charge, and h is the Planck's constant. Thus the average NMR frequency shift ν_Q provides a direct measure of the average strain, while ST linewidth $\Delta\nu_Q$ gives a measure of strain distribution within the quantum dot.

In disk-shaped (large lateral and small vertical dimensions) self-assembled InGaAs/GaAs quantum dots the biaxial strain is positive (tensile along Oz axis).⁴⁵ In such dots negative ν_Q was found for ^{75}As nuclei, implying $S_{11} < 0$. For GaAs/AlGaAs NFDE QDs type A we find positive ν_Q , hence the strain derived from Eq. 1 is negative (compressive along Oz) $\epsilon_b = -0.014\%$. This, however, is expected for disk-shaped dots since GaAs lattice constant is smaller than that of AlGaAs (as opposed to InGaAs/GaAs pair). By contrast, for QDs type B we find anomalous positive (tensile along Oz) $\epsilon_b = 0.007\%$. Most importantly, we always observe either distinctly positive (QDs type B) or distinctly negative (QDs type A) ϵ_b . This allows us to conclude that there is no significant overlap between the excitonic wavefunctions in dots type A and B, as such overlap would have resulted in gradual transition between tensile and compressive strains leading to large inhomogeneous broadening of NMR spectra (as observed in self-assembled dots²²).

The NMR data can be explained consistently if we assume the structure of the dots is as it is shown in Fig. 1(b) and in Fig. 4(c): while QDs type A are formed by in-filling of the nanohole,

the "mounds" formed at the rim of the nanohole (and previously observed in AFM¹⁸) create additional confinement potential resulting in formation of QDs type B. The tensile strain in QDs type B can be explained by the "sloped" AlGaAs barriers resulting in compressive in-plane strain of GaAs as shown with arrows in Fig. 4(c). By contrast the topology of QDs type A in the nanohole is closer to that of a quantum well, so that both AlGaAs barriers act to stretch the GaAs layer in the horizontal plane resulting in compressive strain along Oz ($\epsilon_b < 0$). However, estimating the strain in an ideal GaAs/Al_{0.4}Ga_{0.6}As quantum well⁴⁶ at low temperature gives much lower $\epsilon_b = -0.1\%$. This suggests that in QDs A and B there is a significant degree of in-plane compression resulting most likely from the concave shapes of the dots.

Despite its small magnitude the residual strain has a major impact on the nuclear spin system. From the measurements of the nuclear spin depolarization in the dark, we observe decay times of up to 1000 s in both QDs type A and B. This is significantly longer than in natural fluctuation GaAs/AlGaAs dots where decay times of ~ 40 s were found,³⁷ and is comparable to the decay times in self-assembled InP⁴⁷ and InGaAs⁴⁸ QDs. The enhanced stability of the nuclear spin polarization in the NFDE dots can be understood from the NMR spectra in Figs. 4(a,b): unlike in fluctuation dots,^{49,50} the ST and CT transitions are well resolved, so that the spin exchange between the adjacent nuclei is significantly inhibited. As a result nuclear spin diffusion out of the dot is suppressed providing excellent stability of the nuclear spin magnetization, crucial for achieving long electron and hole spin coherence but found previously only in highly strained self-assembled dots.

In conclusion, we have explored *in situ* nanohole infilled droplet epitaxial quantum dot system with respect to electron and hole spin properties and nuclear spin environment. Investigations into the Landé g -factors have demonstrated a quantum dot system with electron g -factor g_e approaching zero, making it an exciting platform for fully-scalable electric spin control schemes based on g -factor manipulation. Nuclear spin bath can be manipulated optically with polarization degrees as large as 60 % achieved reliably. Structural analysis using NMR spectroscopy reveals small residual strain

that switches from tensile to compressive depending on the type of the dot and leads to very long nuclear spin lifetimes providing a stable spin bath environment for the electron or hole spin.

Acknowledgement The authors are grateful to Armando Rastelli and Yongheng Huo (Linz) for the fruitful discussions. This work has been supported by the EPSRC Programme Grant EP/J007544/1 and the Royal Society. E.A.C. was supported by a University of Sheffield Vice-Chancellor's Fellowship.

References

- (1) Kloeffel, C.; Loss, D. *Annual Review of Condensed Matter Physics* **2013**, *4*, 51–81.
- (2) Gywat, O.; Krenner, H. J.; Berezovsky, J. *Spins in Optically Active Quantum Dots*, 1st ed.; Wiley-VCH, 2010.
- (3) Khaetskii, A. V.; Loss, D.; Glazman, L. *Phys. Rev. Lett.* **2002**, *88*, 186802.
- (4) Merkulov, I. A.; Efros, A. L.; Rosen, M. *Phys. Rev. B* **2002**, *65*, 205309.
- (5) Coish, W. A.; Loss, D. *Phys. Rev. B* **2004**, *70*, 195340.
- (6) Bracker, A. S.; Stinaff, E. A.; Gammon, D.; Ware, M. E.; Tischler, J. G.; Shabaev, A.; Efros, A. L.; Park, D.; Gershoni, D.; Korenev, V. L.; Merkulov, I. A. *Phys. Rev. Lett.* **2005**, *94*, 047402.
- (7) Urbaszek, B.; Braun, P.-F.; Amand, T.; Krebs, O.; Belhadj, T.; Lemaître, A.; Voisin, P.; Marie, X. *Phys. Rev. B* **2007**, *76*, 201301.
- (8) Reilly, D. J.; Taylor, J. M.; Petta, J. R.; Marcus, C. M.; Hanson, M. P.; Gossard, A. C. *Science* **2008**, *321*, 817–821.
- (9) Issler, M.; Kessler, E. M.; Giedke, G.; Yelin, S.; Cirac, I.; Lukin, M. D.; Imamoglu, A. *Phys. Rev. Lett.* **2010**, *105*, 267202.

- (10) Press, D.; De Greve, K.; McMahon, P. L.; Ladd, T. D.; Friess, B.; Schneider, C.; Kamp, M.; Höfling, S.; Forchel, A.; Yamamoto, Y. *Nat Photon* **2010**, *4*, 367–370.
- (11) De Greve, K.; McMahon, P. L.; Press, D.; Ladd, T. D.; Bisping, D.; Schneider, C.; Kamp, M.; Worschech, L.; Höfling, S.; Forchel, A.; Yamamoto, Y. *Nat Phys* **2011**, *7*, 872 – 878.
- (12) Kato, Y.; Myers, R. C.; Driscoll, D. C.; Gosard, A. C.; Levy, J.; Awschalom, D. D. *Science* **2003**, *299*, 1201–1204.
- (13) Pingnot, J.; Pryor, C. E.; Flatté, M. E. *Applied Physics Letters* **2008**, *92*, 222502.
- (14) Pingnot, J.; Pryor, C. E.; Flatté, M. E. *Phys. Rev. B* **2011**, *84*, 195403.
- (15) Belhadj, T.; Kuroda, T.; Simon, C.-M.; Amand, T.; Mano, T.; Sakoda, K.; Koguchi, N.; Marie, X.; Urbaszek, B. *Phys. Rev. B* **2008**, *78*, 205325.
- (16) Abbarchi, M.; Kuroda, T.; Mano, T.; Sakoda, K.; Gurioli, M. *Phys. Rev. B* **2010**, *81*, 035334.
- (17) Sallen, G.; Kunz, S.; Amand, T.; Bouet, L.; Kuroda, T.; Mano, T.; Paget, D.; Krebs, O.; Marie, X.; Sakoda, K.; Urbaszek, B. *Nat Commun* **2014**, *5*, 3268.
- (18) Atkinson, P.; Zallo, E.; Schmidt, O. G. *Journal of Applied Physics* **2012**, *112*, 054303.
- (19) Huo, Y. H.; Rastelli, A.; Schmidt, O. G. *Appl Phys Lett* **2013**, *102*, 152105.
- (20) Gao, W. B.; Imamoglu, A.; Bernien, H.; Hanson, R. *Nat Photon* **2015**, *9*, 363–373.
- (21) Akopian, N.; Wang, L.; Rastelli, A.; Schmidt, O. G.; Zwiller, V. *Nat Photon* **2011**, *5*, 230 – 233.
- (22) Chekhovich, E.; Kavokin, K.; Puebla, J.; Krysa, A.; Hopkinson, M.; Andreev, A.; Sanchez, A.; Beanland, R.; Skolnick, M.; Tartakovskii, A. *Nat Nano* **2012**, *7*, 646–650.
- (23) Bayer, M.; Ortner, G.; Stern, O.; Kuther, A.; Gorbunov, A. A.; Forchel, A.; Hawrylak, P.; Fafard, S.; Hinzer, K.; Reinecke, T. L.; Walck, S. N.; Reithmaier, J. P.; Klopff, F.; Schäfer, F. *Phys. Rev. B* **2002**, *65*, 195315.
- (24) Poem, E.; Kodriano, Y.; Tradonsky, C.; Lindner, N. H.; Gerardot, B. D.; Petroff, P. M.; Gershoni, D. *Nat Phys* **2010**, *6*, 993 – 997.
- (25) Puebla, J.; Chekhovich, E. A.; Hopkinson, M.; Senellart, P.; Lemaître, A.; Skolnick, M. S.; Tartakovskii, A. I. *Phys. Rev. B* **2013**, *88*, 045306.
- (26) Gammon, D.; Efros, A. L.; Kennedy, T. A.; Rosen, M.; Katzer, D. S.; Park, D.; Brown, S. W.; Korenev, V. L.; Merkulov, I. A. *Phys. Rev. Lett.* **2001**, *86*, 5176–5179.
- (27) Janssens, K. L.; Peeters, F. M.; Schweigert, V. A. *Phys. Rev. B* **2001**, *63*, 205311.
- (28) Mano, T.; Abbarchi, M.; Kuroda, T.; McSkimming, B.; Ohtake, A.; Mitsuishi, K.; Sakoda, K. *Applied Physics Express* **2010**, *3*, 065203.
- (29) Snelling, M. J.; Blackwood, E.; McDonagh, C. J.; Harley, R. T.; Foxon, C. T. B. *Phys. Rev. B* **1992**, *45*, 3922–3925.
- (30) Pryor, C. E.; Flatté, M. E. *Phys. Rev. Lett.* **2006**, *96*, 026804.
- (31) Hannak, R. M.; Oestreich, M.; Heberle, A. P.; Rußhler, W. W.; Köhler, K. *Solid State Communications* **1995**, *93*, 313–317.
- (32) White, A.; Hinchliffe, I.; Dean, P.; Greene, P. *Solid State Communications* **1972**, *10*, 497 – 500.
- (33) Kosaka, H.; Kiselev, F. A., A. A. Baron; Kim, K. W.; Yablonovitch, E. *Electronics Letters* **2001**, *37*, 464–465.
- (34) Mejía-Salazar, J. R.; Porrás-Montenegro, N.; Oliveira, L. E. *Journal of Physics: Condensed Matter* **2009**, *21*, 455302.

- (35) Jovanov, V.; Eissfeller, T.; Kapfinger, S.; Clark, E. C.; Klotz, F.; Bichler, M.; Keizer, J. G.; Koenraad, P. M.; Abstreiter, G.; Finley, J. J. *Phys. Rev. B* **2011**, *83*, 161303.
- (36) Bennett, A. J.; Pooley, M. A.; Cao, Y.; Skoeld, N.; Farrer, I.; Ritchie, D. A.; Shields, A. J. *Nat Commun* **2013**, *4*, 1522.
- (37) Nikolaenko, A. E.; Chekhovich, E. A.; Makhonin, M. N.; Drouzas, I. W.; Van'kov, A. B.; Skiba-Szymanska, J.; Skolnick, M. S.; Senellart, P.; Martrou, D.; Lemaître, A.; Tartakovskii, A. I. *Phys. Rev. B* **2009**, *79*, 081303.
- (38) Lai, C. W.; Maletinsky, P.; Badolato, A.; Imamoglu, A. *Phys. Rev. Lett.* **2006**, *96*, 167403.
- (39) Latta, C.; Högele, A.; Zhao, Y.; Vamivakas, A. N.; Maletinsky, M.; Kroner, M.; Dreiser, J.; Carusotto, I.; Badolato, A.; Schuh, D.; Wegscheider, W.; Atature, M.; Imamoglu, A. *Nat Phys* **2009**, *5*, 758 – 763.
- (40) Kloeffel, C.; Dalgarno, P. A.; Urbaszek, B.; Gerardot, B. D.; Brunner, D.; Petroff, P. M.; Loss, D.; Warburton, R. J. *Phys. Rev. Lett.* **2011**, *106*, 046802.
- (41) Högele, A.; Kroner, M.; Latta, C.; Claassen, M.; Carusotto, I.; Bulutay, C.; Imamoglu, A. *Phys. Rev. Lett.* **2012**, *108*, 197403.
- (42) Kessler, C. A.; Reischle, M.; Roßbach, R.; Koroknay, E.; Jetter, M.; Schweizer, H.; Michler, P. *physica status solidi (b)* **2012**, *249*, 747–751.
- (43) Urbaszek, B.; Marie, X.; Amand, T.; Krebs, O.; Voisin, P.; Maletinsky, P.; Hoegel, A.; Imamoglu, A. *Rev. Mod. Phys.* **2013**, *85*, 79–133.
- (44) Sundfors, R. K. *Phys. Rev. B* **1974**, *10*, 4244–4252.
- (45) Pearson, G. S.; Faux, D. A. *Journal of Applied Physics* **2000**, *88*.
- (46) Grundmann, M.; Stier, O.; Bimberg, D. *Phys. Rev. B* **1995**, *52*, 11969–11981.
- (47) Chekhovich, E. A.; Makhonin, M. N.; Skiba-Szymanska, J.; Krysa, A. B.; Kulakovskii, V. D.; Skolnick, M. S.; Tartakovskii, A. I. *Phys. Rev. B* **2010**, *81*, 245308.
- (48) Maletinsky, P.; Kroner, M.; Imamoglu, A. *Nat Phys* **2009**, *5*, 407 – 411.
- (49) Gammon, D.; Brown, S. W.; Snow, E. S.; Kennedy, T. A.; Katzer, D. S.; Park, D. *Science* **1997**, *277*, 85–88.
- (50) Makhonin, M. N.; Chekhovich, E. A.; Senellart, P.; Lemaître, A.; Skolnick, M. S.; Tartakovskii, A. I. *Phys. Rev. B* **2010**, *82*, 161309.

Graphical TOC Entry

